



Research article

Motion and trajectory planning modeling for mobile landing mechanism systems based on improved genetic algorithm

Jinhua Zhou, Shan Jia*, Jinbao Chen and Meng Chen

College of Aerospace Engineering, Nanjing University of Aeronautics and Astronautics, Nanjing 210016, China

* Correspondence: Email: jiashanazz@nuaa.edu.cn.

Abstract: In many traditional soft-landing missions, researchers design the lander and the rover as two separate individuals, which has its limitations. At present, research on landers mainly focuses on the performance analysis of those who cannot move, and the motion of legged mobile lander has not yet been studied. In this paper, a novel Mobile Landing Mechanism (MLM) is proposed. Firstly, the monte-Carlo method is used to solve the workspace, and the motion feasibility of the mechanism is verified. Secondly, combining with the constraints of velocity, acceleration and secondary acceleration of each driving joint of the MLM, the trajectory of its joint space is planned by using cubic spline curve. And based on the weighted coefficient method, an optimal time-jerk pedestal trajectory planning model is established. Finally, by comparing the genetic algorithm (GA) with the adaptive genetic algorithm (AGA), an optimization algorithm is proposed to solve the joint trajectory optimization problem of the MLM, which can obtain better trajectory under constraints. Simulation shows that the motion performance of the mechanism is continuous and stable, which proves the rationality and effectiveness of the foot trajectory planning method.

Keywords: mobile landing mechanism (MLM); cubic spline curve; trajectory planning; adaptive genetic algorithm (AGA)

1. Introduction

Lander and rover played a vital role in landing exploration, in previous missions [1], many different types of landers and rovers were launched onto the surface of the moon and other planets. Nowadays, with the increasing requirements of landing detection technology, the lander also needs to have more functions. In the past few decades, many important models have been developed, such as Luna 16 [2,3], Euro Moon 2000 [4], Altair Lander [5], The Insight Mars Lander [6], Chang e 4 [7], etc.. Most of them have four legs, each of which consists of a main buffer mechanism, an auxiliary buffer mechanism and a foot pad, can be folded and then unfolded, and absorbs shock on impact. However, it is not possible of them to realize functions like attitude adjustment and walking (or moving). Therefore, detection tasks, though very limited, cannot be accomplished without the aid of rover.

In order to expand the detection range of the extra-terrestrial galaxies' surface, some movable rovers with wheeled mechanisms have been developed, such as Sojourner rover [8], Mars Rover mission [9] Spirit and Opportunity rovers, Jade Rabbit rover [10] and so on. However, most wheeled rovers have limited ability to travel through complex and harsh terrain environments, and even basic functions like moving and adjusting directions are impossible.

The rover must be carried to the surface of the extra-terrestrial galaxies by the lander before the subsequent detection mission, which has some limitations [11–14]: (1) The explore range of motion of the rover is very limited. The rover cannot reach remote destinations remote from the landing site since they have to receive energy and other supplies from the lander after extravehicular activity, which means, even both lander and rover can keep working without damage, it is still impossible of the rover to explore areas beyond a certain safe range. (2) As the exploration mission became more complex, it will be a great challenge for the wheeled rover to pass through rough terrains full of obstacles and slopes.

To solve problems above, a novel legged mobile landing mechanism is in urgent need. At present, some configurations of the legged mobile lander have been proposed. However, they are still in stages of conception, and no in-depth study on their walking characteristics and trajectory planning is ever conducted. One key issue of designing such a lander is to design the structure of its leg, which should bear high payload and have high reliability at the same time. To cope with such demands, the parallel configuration is considered to be a good choice. Parallel mechanisms have been widely used in aircraft simulators, force/torque sensors and acceleration sensors [15,16]. In recent years, parallel mechanisms that both maintain the inherent advantages of parallel mechanisms and possess several other advantages in terms of the total cost reduction in manufacturing and wider workspace (the Delta robot [17], and Tricept robot and Trivariant robot [18]), are drawing increasing attention of researchers. Combined with the traditional parallel robot configuration features, and combine parallel robots with traditional lander configurations, such as PH-Robot [19], Prototypes of Octopus robot [20], and so on.

A novel design for the kinematic control structure of the wheeled mobile robot (WMR) path planning and path-following was presented [21]. A mobile robot path planning method in the visualize plane using an overhead camera based on interval type-2 fuzzy logic (IT2FIS) was proposed. It is necessary to determine the location of a mobile robot in an environment surrounding the robot [22]. The Mem-PBPF algorithm yields improved performance in terms of time execution by using a parallel implementation on a multi-core computer was proposed. Therefore, the Mem-PBPF algorithm achieves

high performance yielding competitive results for autonomous mobile robot navigation in complex and real scenarios [23]. A novel proposal makes use of the Artificial Potential Field (APF) method with a Bacterial Evolutionary Algorithm (BEA) to obtain an enhanced flexible path planner method taking all the advantages of using the APF method, strongly reducing its disadvantages [24]. A navigation software called Ant Colony Test Center designed to teach the different stages involved in mobile robotics was presented [25]. A novel proposal to solve the problem of path planning for mobile robots based on Simple Ant Colony Optimization Meta-Heuristic (SACO-MH) was presented [26].

In this paper, we focus on type synthesis of an innovative legged mobile lander combining characteristics and capabilities of both the lander and the rover inspired by the configurations of existing landers and walking robots. The MLM works as a landing buffer during landing. After that, it has 3 working modes: in mode 1, the stationary legged mobile lander works as a base camp; in mode 2, it performs exploratory tasks using its legs, which can be seen as a legged rover; while in mode 3, the MLM adjust its attitude to prepare for launching.

The purpose of designing the MLM is to ensure that the lander has good motion stability and environmental adaptation. One of the difficulties in lander motion control is to optimize the foot motion trajectory of the MLM [27,28]. Researchers have made achievements on the problem. (Y-sway and E-sway motions [29,30], a sinusoidal sway [31] and the trajectory planning method based on the quantic spline curve [32]). However, few attentions have been paid to methods of foot trajectory planning for quadruped parallel robots. When performing a walking task, the leg structure will inevitably produce an obvious mechanical vibration, which will greatly jeopardize the walking stability of the whole machine. To solve such problems, by taking characteristics of configuration and motion into consideration, a method of trajectory planning for the foot is proposed.

At present, the research direction in the field of robot research mainly dedicated to the study of trajectory planning, under certain conditions this also to solve nonlinear constrained optimization problem provides a new train of thought Liu et al. [33] proposed a time optimal rapid continuous motion constraints, robot trajectory planning method in order to solve the problem of the optimal trajectory planning of robot, Xu et al. [34] put forward a kind of environment - genetic evolution immune clone algorithm Liu et al. [35] weighting coefficient method is used to establish the industrial robot trajectory planning model, and puts forward an improved adaptive genetic algorithm to solve Saramago and Steffen [36] solved the problem of manipulator moving at the minimum cost on the specified geometric path. Since the working environment of MLM studied in this paper is different from that of industrial robots, not only efficiency but also stability should be considered. The acceleration of impact force can be effectively controlled by controlling impact.

This paper is organized as follows, after discussing the structure configuration in sections I, the kinematics of the MLM is studied and analyzed in section II. The optimal time-jerk trajectory planning method is proposed in section III. Simulation and experiment results and discussions are presented in section IV. Finally, conclusions are given in section V.

2. Description of the MLM

In this paper, the MLM is a parallel mechanism, as shown in Figure 1(a), R, U, P, and S denote revolute, universal, prismatic and spherical joint respectively. P pair is the actuated joint driven by an

actuator. The MLM's structure includes: main body, swinging limb, RPR limb, upper leg, UPS limb-1, UPS limb-2, ball joint mounting bracket and foot. One end of the swinging limb is connected to the main body by a revolute joint, and the other connected to the upper leg by a Hooke joint. The middle position of the swinging limb is connected with the RPR limb by a revolute joint. The other end of the RPR limb is connected to the main body by a revolute joint, and the linear actuator installed on the RPR limb provides power for the swing rod installed on the body to swing up and down. The ball joint bearing is installed at the lower end of the upper leg. The two UPS limbs are of the same structure, whose one end is connected to the main body by a Hook joint, and the other connected to the ball joint mounting bracket on the upper leg by a ball joint. The middle part is the linear actuator.

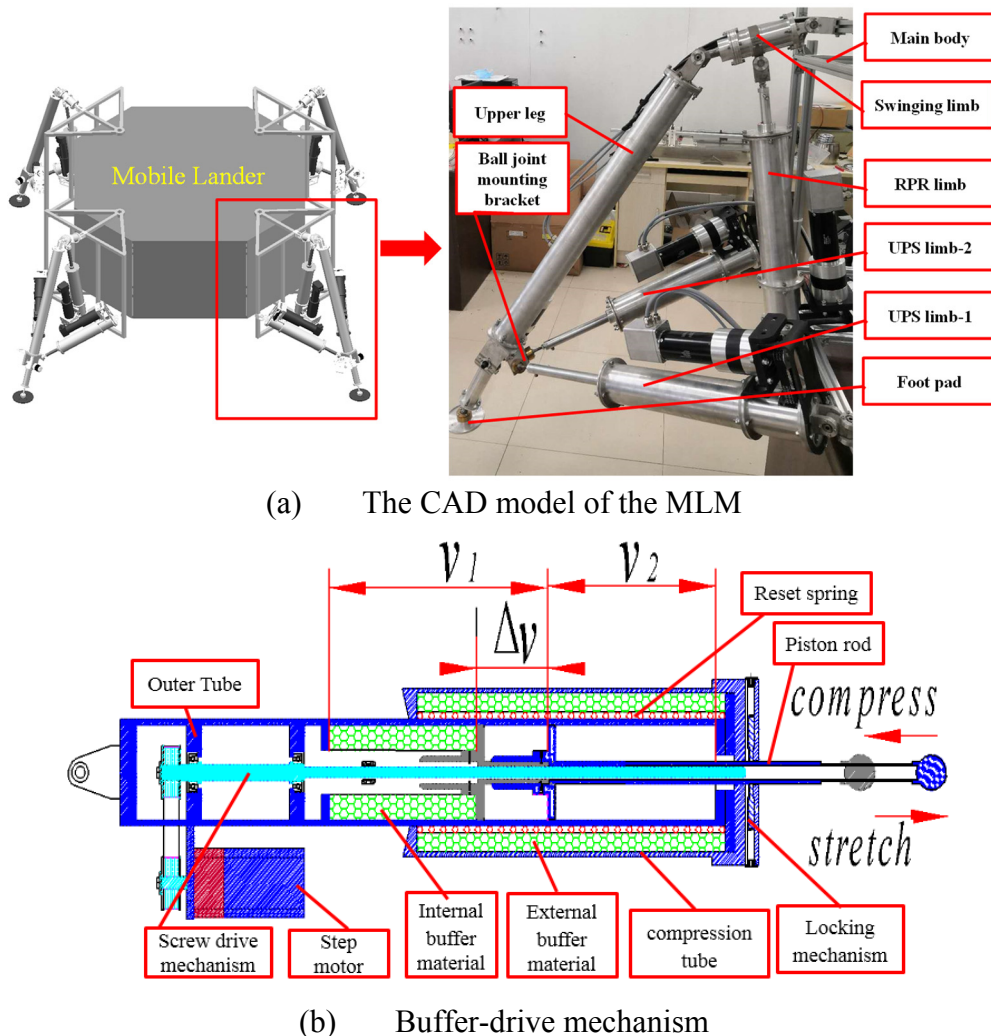


Figure 1. Schematic diagram of the MLM.

The MLM is composed of three groups of buffer-drive mechanism, as shown in Figure 1(b). The buffer drive mechanism is mainly composed of the outer tube, compression tube, internal buffer materials, external buffer materials, piston rod, locking mechanism, screw drive mechanism, step motor and reset spring. Due to the complexity of landing environment, buffer-drive mechanism may be stretched or compressed during landing impact. When compressed, the internal buffer material is

compressed by the piston rod. When stretched, the external buffer material is compressed by the piston rod through the locking mechanism and the outer tube. Since the compression length of the external buffer material does not affect the motion performance of MLM, only the compressed state of the internal buffer material is considered. Before compression, the initial distance of the internal buffer material is v_1 . Piston rod can move distance is v_2 . After compression, buffer material compression distance is Δv . At this point, the piston rod can move distance is $\Delta v + v_2$. Internal critical compression of the buffer to the distance is $\Delta v = 0$ and $\Delta v = v_1$. Therefore, in order to ensure the safety and feasibility of MLM mechanism. v_2 is used as the input conditions of the workspace.

3. Kinematics and workspace analysis

3.1. Kinematics

Figure 2 shows the schematic diagram of the MLM, which can be decomposed into eight isolated rigid bodies. U_i ($i=1,2,3$) denotes the center of the U joint. s_i ($i=2,3$) denotes the center of the S joint. A denotes the end point of the upper leg. The point O_S is the intersection of the upper leg and the normal plane on which points O_S , s_2 and s_3 are located. $\Delta R_0 U_2 U_3$ and $\Delta O_s S_2 S_3$ are isosceles triangles. Frame $R_0 - x_0 y_0 z_0$ is fixed on the main body, while z_0 axis coincides with the first rotational axis of R_0 , R_0 axis is parallel to both, R_1 axis and R_2 axis. z_2 axis and z_3 axis intersect at origin U_1 and are perpendicular to each other. At O_s , the upper leg is perpendicular to the plane where $\Delta O_s S_2 S_3$ lies limb $U_2 P_2 S_2$ is connected to s_2 on $\Delta O_s S_2 S_3$. Similarly, limb $U_3 P_3 S_3$ is connected to S_3 on $\Delta O_s S_2 S_3$. B_1 denotes the distance between point R_0 and U_1 . B_2 denotes the distance between point O_4 and U_1 , and d denotes the distance between the tip A and point O_4 . $L_1 \equiv \overline{R_2 R_1}$, $L_2 \equiv \overline{U_2 S_2}$ and $L_3 \equiv \overline{U_3 S_3}$ are defined as components in the base frame $R_0 - x_0 y_0 z_0$.

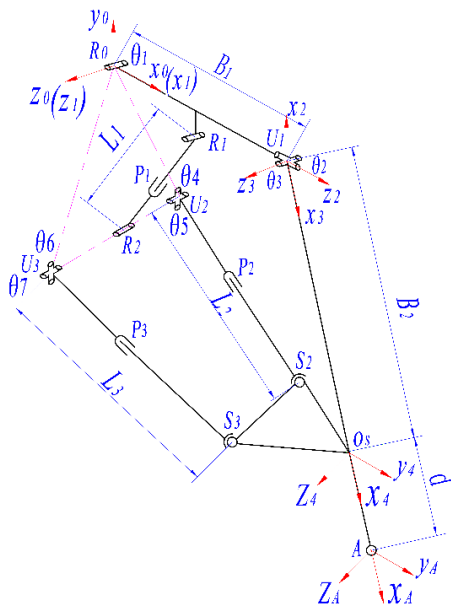


Figure 2. Schematic diagram of the MLM.

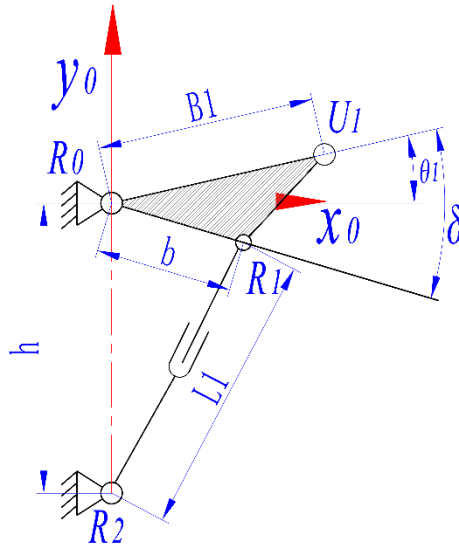


Figure 3. Schematic diagram of swinging limb movement.

Firstly, as usual, the relationship between the position of point O_S at the tip and the position of the MLM should be derived to implement trajectory tracking. The three limbs in the MLM are $R_0U_1O_SA$, $U_2P_2S_2$ and $U_3P_3S_3$. Firstly, the frames are established at each revolute joint position of the limb $R_0U_1O_SA$ by the D-H method [37]. We can obtain the transformation matrix between adjacent link-fixed frames between frames $R_0 - x_0y_0z_0$ and $O_S - x_4y_4z_4$, as follows:

$${}^{i-1}\mathbf{T}_i = \begin{bmatrix} {}^{i-1}\mathbf{R} & {}^{i-1}\mathbf{P} \\ 0 & 1 \end{bmatrix} \quad (1)$$

where,

$${}^{i-1}\mathbf{R} = \begin{bmatrix} \cos\theta_i & -\sin\theta_i \cos\omega_{i-1} & \sin\theta_i \sin\omega_{i-1} \\ \sin\theta_i & \cos\theta_i \cos\omega_{i-1} & -\cos\theta_i \sin\omega_{i-1} \\ 0 & \sin\omega_{i-1} & \cos\omega_{i-1} \end{bmatrix} \quad (2)$$

$${}^{i-1}\mathbf{P} = \begin{bmatrix} d_{i-1} \cos\theta_i \\ d_{i-1} \sin\theta_i \\ a_i \end{bmatrix} \quad (3)$$

a_i is the distance from z_i to z_{i+1} along the x_i , w_i is the rotation angle from z_i to z_{i+1} around x_i , θ_i is the rotation angle from x_{i-1} to x_i around z_i , d_i is the distance from x_{i-1} to x_i along the z_i .

We solve the kinematic equations as follows. In deriving the kinematic equations for the MLM, we formed the transformation matrix between frame R_0 and O_S :

$${}^0T_4 = {}^0T_1^1 {}^1T_2^2 {}^2T_3^3 {}^3T_4 = \begin{pmatrix} C_1C_2C_3 - S_1S_3 & -C_3S_1 - C_1C_2S_3 & -C_1S_2 & -B_2(S_1S_3 - C_1C_2C_3) \\ C_1S_3 + C_2C_3S_1 & C_1C_3 - C_2S_1S_3 & -S_1S_2 & B_2(C_1S_3 + C_2C_3S_1) - B_1C_1 \\ C_3S_2 & -S_2S_3 & C_2 & B_2C_3S_2 \\ 0 & 0 & 0 & 1 \end{pmatrix} \quad (4)$$

Where S_i and C_i ($i=1,2,3$) denote $\sin \theta_i$ and $\cos \theta_i$, respectively. Then, the position vector of tip A in frame $R_0 - x_0 y_0 z_0$ can be derived,

$${}^0T_A = \begin{pmatrix} 0 \\ 0 \\ 0 \end{pmatrix} = \begin{pmatrix} B_1S_1 - (B_2 + d)(S_1S_3 - C_1C_2C_3) \\ (B_2 + d)(C_1S_3 + C_2C_3S_1) - B_1C_1 \\ (B_2 + d)C_3S_2 \end{pmatrix} \quad (5)$$

From Figure 3 and Eq (5), the following equation is obtained,

$$\begin{cases} \theta_1 = \arcsin\left(\frac{Ax^2 + Ay^2 + Az^2 - (B_2 + d)^2}{2B_1\sqrt{Ax^2 + Ay^2}}\right) + \arctan\left(\frac{Ay}{Ax}\right) \\ \theta_2 = \arctan\left(\frac{-2B_1Az}{\sqrt{4B_1^2 + (Ax^2 + Ay^2) - (Ax^2 + Ay^2 + Az^2 + B_1^2 - (B_2 + d)^2)^2}}\right) \\ \theta_3 = \pi - \arcsin\left(\frac{(B_2 + d)^2 - (Ax^2 + Ay^2 + Az^2)}{2B_1(B_2 + d)}\right) \end{cases} \quad (6)$$

$$L_1 = \sqrt{h^2 + b^2 - 2hb\cos\left(\theta_1 + \frac{\pi}{2} - \delta\right)} \quad (7)$$

From the geometrical relationship and Figure 2, we obtained:

$$\begin{cases} \begin{bmatrix} \mathbf{L}_2 \\ 0 \end{bmatrix} = {}^0T_4 \begin{bmatrix} 1 \\ 1 \end{bmatrix} - \begin{bmatrix} {}^0\mathbf{P}_{S2} \\ 1 \end{bmatrix} \\ \begin{bmatrix} \mathbf{L}_3 \\ 0 \end{bmatrix} = {}^0T_4 \begin{bmatrix} 1 \\ 1 \end{bmatrix} - \begin{bmatrix} {}^0\mathbf{P}_{S3} \\ 1 \end{bmatrix} \end{cases} \quad (8)$$

Where,

$${}^0\mathbf{P}_{U2} = \begin{bmatrix} 0 \\ -ay \\ -az \end{bmatrix}, {}^0\mathbf{P}_{U3} = \begin{bmatrix} 0 \\ -ay \\ az \end{bmatrix}, {}^0\mathbf{P}_{S2} = \begin{bmatrix} 0 \\ -by \\ -bz \end{bmatrix}, {}^0\mathbf{P}_{S3} = \begin{bmatrix} 0 \\ -by \\ bz \end{bmatrix}.$$

It can be derived from Eqs (5)–(8).

$$\begin{cases} \mathbf{L}_2 = \begin{bmatrix} by(C_3S_1 + C_1C_2C_3) - B_2(S_1S_3 - C_1C_2C_3) + B_1S_1 + bzC_1S_2 \\ ay + B_2(C_1S_3 + C_2C_3S_1) - by(C_1C_3 - C_2S_1S_3) - B_1C_1 + bzS_1S_2 \\ az - bzC_2 + B_2C_3S_2 + byS_2S_3 \end{bmatrix} \\ \mathbf{L}_3 = \begin{bmatrix} by(C_3S_1 + C_1C_2C_3) - B_2(S_1S_3 - C_1C_2C_3) + B_1S_1 - bzC_1S_2 \\ ay + B_2(C_1S_3 + C_2C_3S_1) - by(C_1C_3 - C_2S_1S_3) - B_1C_1 - bzS_1S_2 \\ bzC_2 - az - bzC_2 + B_2C_3S_2 + byS_2S_3 \end{bmatrix} \end{cases} \quad (9)$$

Thus, the displacements of \mathbf{L}_2 and \mathbf{L}_3 can be represented as :

$$\begin{cases} L_2 = \sqrt{\mathbf{L}_2^T \mathbf{L}_2} \\ L_3 = \sqrt{\mathbf{L}_3^T \mathbf{L}_3} \end{cases} \quad (10)$$

3.2. Workspace analysis

3.2.1. Constraints

The size and shape of the reachable workspace of the foot end is constrained by the following factors: (1) length of the limb; (2) limitation of universal joint. The constraints can be expressed as follows:

$$\begin{cases} L_{i\min} < L_i < L_{i\max} \\ \theta_i < \theta_{i\max} \end{cases} \quad (11)$$

where θ_i is real angle of the universal joint; $\theta_{i\max}$ is the allowable maximal angle of the universal joint; $L_{i\min}$ is the minimum of the limb length; $L_{i\max}$ is the maximum of the limb length.

Table 1 shows parameters of dimension and kinematic pairs of the MLM.

Table 1. Parameters of dimension and kinematic pairs of the MLM.

No.	Parameter	Value
1	L_1 /mm	600 ~ 960
2	L_2 /mm	580 ~ 780
3	L_3 /mm	580 ~ 780
4	θ_1 / °	-5 ~ 30
5	θ_2 / °	-20 ~ 20
6	θ_3 / °	-60 ~ -90
7	B_1 /mm	500
8	B_2 /mm	2093
9	d/mm	500

3.2.2. Reachable Workspace of MLM

Referring to the constraints in Table 1, the reachable workspace of the foot end can be solved by Monte Carlo method [38], as shown in Figure 4.

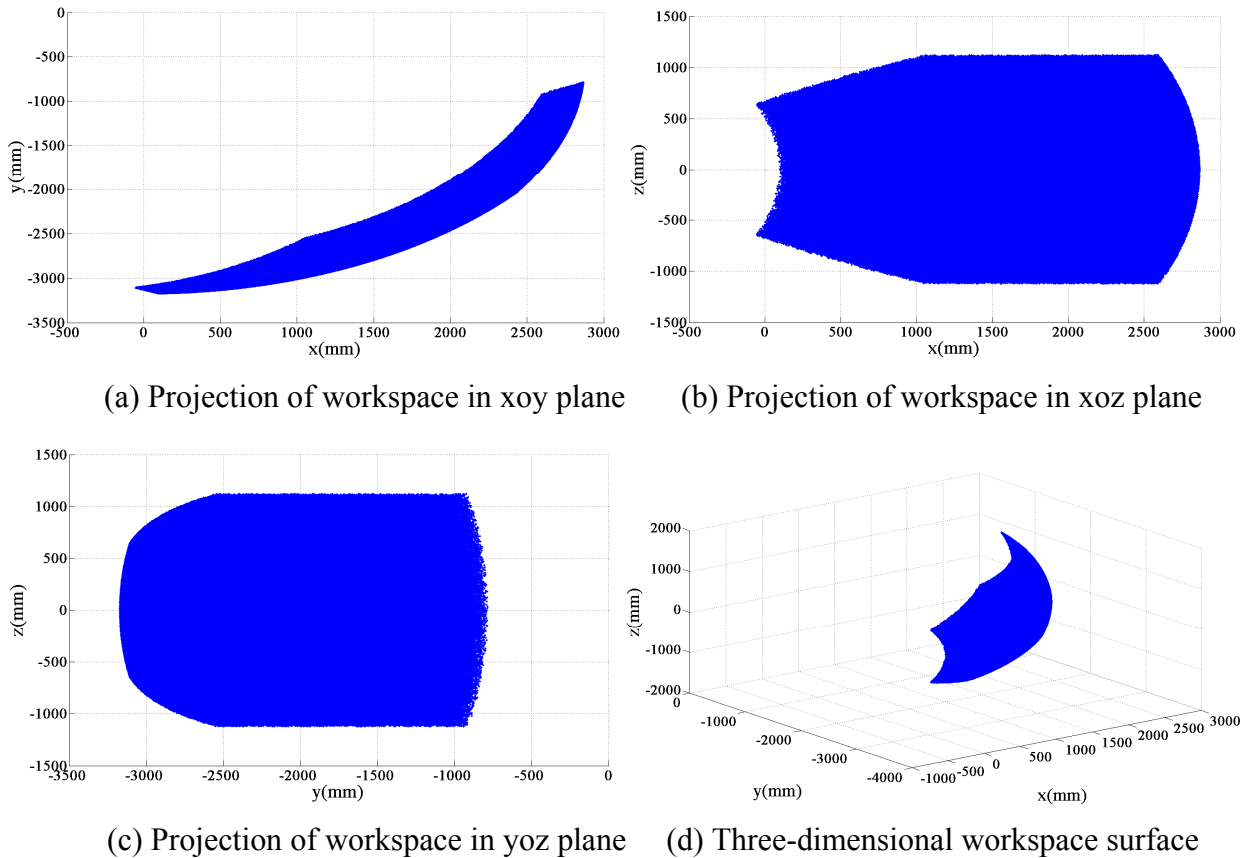


Figure 4. Reachable workspace of the foot end.

In Figure 4 it can be found that the value and fluctuate for the foot end is smaller when the reachable workspace is in the ranges $x \in [-50 \sim 2800]$ mm, $y \in [-3200 \sim -750]$ mm, $z \in [-1100 \sim 1100]$ mm, which is reasonably large to walk. Therefore, this area can be chosen as the optimal motion workspace of the leg mechanism.

With the mechanism meeting requirements of walking, its mobility stability becomes particularly important since the lander works in a complex working environment, which requires the end motion trajectory of the mechanism to be optimized.

4. Minimum time-jerk trajectory planning problem

4.1. Construction of the end trajectory

Joint trajectories of the MLM can be obtained by polynomial or cubic spline method. Those generated by cubic splines have continuous accelerations, comparing with the higher order polynomial method, cubic splines overcome problems like over-oscillation and overshoot between pairs of reference points. The knots in the path of the motion joint in Cartesian space are mapped to joint space [39]. Meanwhile, the cubic spline curve was used to interpolate the knots of each motor joint. We obtained a cubic polynomial that satisfies the following conditions.

$$\begin{aligned} G_{ji}(t) = & \frac{\ddot{G}_{ji}(t_i)}{6h_i}(t_{i+1}-t)^3 + \frac{\ddot{G}_{ji}(t_{i+1})}{6h_i}(t-t_i)^3 + \\ & \left(\frac{g_{ji+1}}{h_i} - \frac{h_i \ddot{G}_{ji}(t_{i+1})}{6}\right)(t-t_i) + \left(\frac{g_{ji}}{h_i} - \frac{h_i \ddot{G}_{ji}(t_i)}{6}\right)(t_{i+1}-t) \end{aligned} \quad (12)$$

$$\begin{aligned} \dot{G}_{ji}(t) = & \frac{\ddot{G}_{ji}(t_i)}{2h_i}(t_{i+1}-t)^2 + \frac{\ddot{G}_{ji}(t_{i+1})}{6h_i}(t-t_i)^2 + \\ & \left(\frac{g_{ji+1}}{h_i} - \frac{h_i \ddot{G}_{ji}(t_{i+1})}{6}\right) + \left(\frac{g_{ji}}{h_i} - \frac{h_i \ddot{G}_{ji}(t_i)}{6}\right) \end{aligned} \quad (13)$$

$$\ddot{G}_{ji}(t) = \frac{t_{i+1}-t}{h_i} \ddot{G}_{ji}(t_i) + \frac{t-t_i}{h_i} \ddot{G}_{ji}(t_{i+1}) \quad (14)$$

$$\ddot{G}_{ji}(t) = \frac{\ddot{G}_{ji}(t_{i+1}) - \ddot{G}_{ji}(t_i)}{h_i} \quad (15)$$

In Eqs (12)–(15), $h_i = t_{i+1} - t_i$, $t \in [t_i, t_{i+1}]$, g_{ji}, v_{ji}, a_{ji} , $i = 1, 2, \dots, n-1$, denote the displacement, instantaneous velocity and instantaneous acceleration of i th key node in j th joint, of which v_{j1}, a_{j1} and v_{jn}, a_{jn} , are given, $j = 1, 2, \dots, N$, $i = 1, 2, \dots, n$; $\{t_1, t_2, \dots, t_n\}$ is the time series of the movement of the MLM to each key point. We also define $G_{ji}(t), \dot{G}_{ji}(t), \ddot{G}_{ji}(t)$ and $\ddot{\ddot{G}}_{ji}(t)$ as the displacement, velocity, acceleration and quadratic acceleration in the time interval $[t_i, t_{i+1}]$ of joint j .

4.2. Constraints

The motion of MLM actuators is constrained by velocity, accelerator and the second accelerator.

4.2.1. Velocity constraints

$$|\dot{G}_{ji}(t)| - V_{jm} \leq 0 \quad (16)$$

With $\dot{G}_{ji}(t)$ being quadratic (13), its maximum can be denoted as $\text{Max} [\dot{G}_{ji}(t_1), \dot{G}_{ji}(t_{i+1}), \dot{G}_{ji}(t_i)]$, that is

$$\text{Max} [\dot{G}_{ji}(t_1), \dot{G}_{ji}(t_{i+1}), \dot{G}_{ji}(t_i)] - V_{jm} \leq 0 \quad (17)$$

4.2.2. Acceleration constraints

$$|\ddot{G}_{ji}(t)| - A_{jm} \leq 0 \quad (18)$$

we then obtain:

$$\text{Max } \left[\left| \ddot{G}_{ji}(t_i) \right|, \left| \dot{G}_{ji}(t_{i+1}) \right| \right] - A_{jm} \leq 0 \quad (19)$$

4.2.3. Jerk constraint

$$\left[\left| \ddot{G}_{ji}(t_i) \right| \right] - J_{jm} \leq 0 \quad (20)$$

4.3. Optimal objective

We notice that quadratic acceleration in Eq (15) is not continuous, namely, there are jerks when the MLM's end moves from the initial position to some desired final position.

Jerks not only accelerate the wear and tear of the parts, but also increase the end-effector positioning errors. As a result, the stability of the whole machine is reduced. In order to make the manipulator satisfied a certain work efficiency, and to ensure the movement is relatively stable, we established a time-jerk optimal trajectory planning model with respect to the total operation time and the square of the jerk for the components, that is:

$$\min \left[W_T N \sum_{i=1}^{n-1} h_i + W_J \sum_{j=1}^N \sum_{i=1}^{n-1} \left(\frac{\left[\ddot{G}_{ji}(t_{i+1}) - \ddot{G}_{ji}(t_i) \right]^2}{h_i} \right) \right] \quad (21)$$

Where W_T denotes the weight of time, W_J denotes the weight of jerk, and $W_T + W_J = 1$. The values of the weights W_T and W_J can be chosen to obtain the minimum time-jerk trajectory to some extent. By choosing $W_J = 0$ a minimum-time trajectory is found, while setting $W_T = 0$ enables one to obtain a minimum-jerk trajectory.

5. Trajectory planning simulation and discussion

5.1. Analysis of algorithms

In order to optimize the Eq (21), we first map the optimized search space to search space of the genetic algorithm (GA), then the optimization parameter and the fitness function was determined. In order to make the optimization problem of objective function conforms to the operation rules of GA. Finally, the optimal objective function value is obtained by time segments. AGA not only can not consider specific meaning of parameters and their complicated relationship, the algorithm can deal with complicated problems, especially some issues of value concept has stronger global searching ability, at the same time as a result of the parallel search method, makes the genetic algorithm has a faster search at the same time also can apply to most, solving nonlinear large peak of discontinuous

function more for function optimization problems show no expression can also apply. An adaptive fitness function is adopted in this paper, which can be automatically adjusted individual fitness gap according to the changes of the individual living environment, making the algorithm converges to its optimal solution. Thus, the blindness of the initial optimization can be greatly reduced, the amount of computation can be saved, and the real-time performance of the algorithm can be improved.

In this paper, the model of minimum time-jerk trajectory planning is presented with cubic splines connected the points. However, this model has the characteristics of complex coupling relationship and strong nonlinearity, so if traditional genetic algorithm is used, it is easy to fall into the local optimal solution. An adaptive fitness function is adopted in this paper, which can be automatically adjusted individual fitness gap according to the changes of the individual living environment, making the algorithm converges to its optimal solution. Thus, the blindness of the initial optimization can be greatly reduced, the amount of computation can be saved, and the real-time performance of the algorithm can be improved.

Specific implementation steps:

5.1.1. Local optimization

A small population with less evolutionary algebra was set up, the local optimal velocity can be obtained quickly. The landing leg structure first runs along the trajectory according to this optimal velocity.

5.1.2. Global optimization

Expand the population and increase the evolutionary algebra so that the global optimal velocity is obtained, ultimately ensuring that the landing leg structure runs at the optimal velocity trajectory.

The individual is selected by the individual's fitness degree, the roulette model is established, and the elite with the smallest probability value is directly replaced and copied to the next generation with the elite selection probability p_s [40].

Crossover and mutation probability affect the individual diversity, robustness and convergence of GA. The sigmoid function of neural network was introduced into GA as an adaptive function of crossover probability and mutation probability, as shown in Eqs (22) and (23).

$$u_c = \begin{cases} \frac{u_{c\max} - u_{c\min}}{1 + \exp\left(A \frac{2(f^* - f_{avg})}{f_{\max} - f_{avg}}\right)}, & f^* - f_{avg} \geq 0, \\ u_{c\max}, & f^* - f_{avg} < 0 \end{cases} \quad (22)$$

$$u_m = \begin{cases} \frac{u_{m\max} - u_{m\min}}{1 + \exp\left(9.903438 \frac{2(f^* - f_{avg})}{f_{\max} - f_{avg}}\right)}, & f^* - f_{avg} \geq 0, \\ u_{m\max}, & f^* - f_{avg} < 0 \end{cases} \quad (23)$$

Where u_c denotes the crossover probability; u_m denotes the mutation probability, $u_{c\max}$ denotes the upper limit of crossover probability contemporary populations; $u_{c\min}$ denotes the lower limit of crossover probability; f^* denotes the value of higher fitness of the two selected individuals; f denotes the fitness value of mutating individual; f_{avg} denotes the average value of contemporary populations; f_{\max} denotes the maximum fitness value of contemporary population; $u_{c\max}$ denotes the upper limit of crossover probability contemporary populations; $u_{m\max}$ denotes the upper limit of mutation probability; $u_{m\min}$ denotes the lower limit of mutation probability.

Eqs (22) and (23) suggested that when the individual fitness values of the population tend to be consistent, larger u_m and u_c are needed. Whereas the population individual fitness values are dispersed, the smaller u_m and u_c are selected. The flow chart of the adaptive genetic algorithm (AGA) is shown in Figure 5.

5.2. Experimental setup

Considering the constraints of landing leg structure parameters and motion parameters, we chose a safe workspace for the simulation experiment. in the ranges $x \in (1000 \sim 2000 \text{ mm})$, $y \in (-3000 \sim -2000 \text{ mm})$ and $z \in (-400 \sim 400 \text{ mm})$. Based on the kinematics equation obtained in part 2, under the premise of displacement, velocity and acceleration of the joint space, the AGA program is designed.

Based on the weighted coefficient method, an optimal time-jerk pedestal trajectory planning model is established. By adjusting different weighting coefficients, the minimum parameters of time and jerk are obtained. The limits of Kinematic Limits are expressed in Table 3, and the displacement of knots in joint space are reported in Table 4. By using the genetic algorithm (GA) for the optimal solution, we obtained the optimal trajectories in various W_r and W_J . As shown in Figure 6, we set the trajectory of the end-effector of the MLM with respect to the inertial reference frame $A-XYZ$ as follows:

Table 2. Parameter settings of hybrid optimization algorithm.

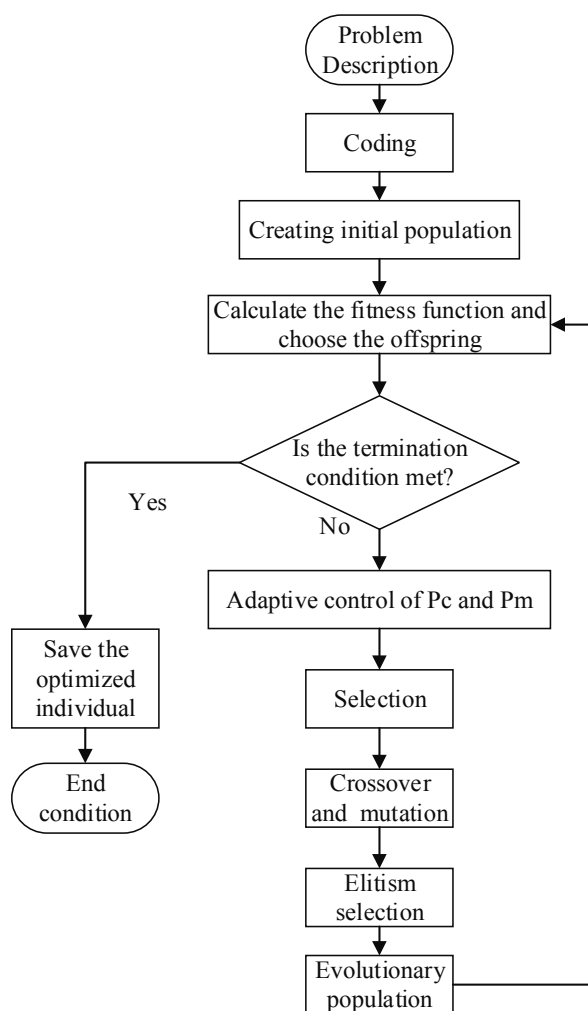
Parameter	Value	Parameter	Value
population size	50	Cross probability $u_{c\min}$	0.8
maximum number of generations	600	Mutation probability $u_{m\max}$	0.2
Cross probability $u_{c\max}$	0.99	Mutation probability $u_{m\min}$	0.05

Table 3. Kinematic Limits of Each joint.

Constraint	Joint		
	1	2	3
Velocity/(deg/s)	400	380	380
Acceleration/(deg/s ²)	200	180	180
Jerk/(deg/s ³)	100	90	90

Table 4. The displacements of knots in joint space.

Knots /deg	Joint		
	1	2	3
g1	15.2102	-16.9058	-14.758
g2	Virtual point	Virtual point	Virtual point
g3	12.6982	-13.3764	-6.8201
g4	9.307	-8.8297	1.6705
g5	5.2752	-3.6047	10.0103
g6	0.8918	1.9217	17.4333
g7	-3.4917	7.25968	23.3867
g8	-7.6867	11.9948	27.4687
g9	-11.4045	15.7754	29.5034
g10	-14.444	18.3502	29.4909
g11	-16.5415	19.6062	27.6194
g12	-17.5212	19.5057	24.0775
g13	-17.1444	18.1618	19.1414

**Figure 5.** Flow diagram of AGA.

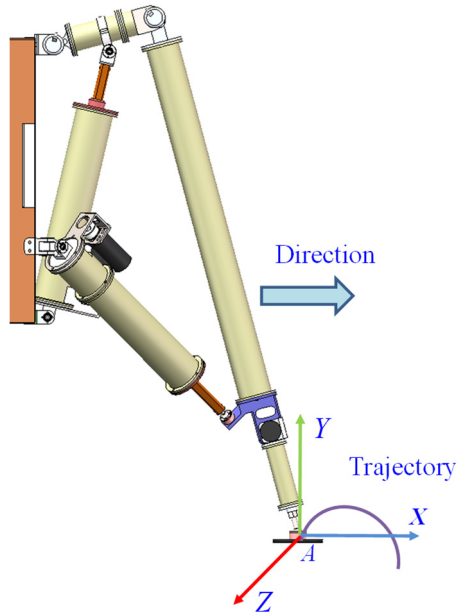


Figure 6. The walking trajectory.

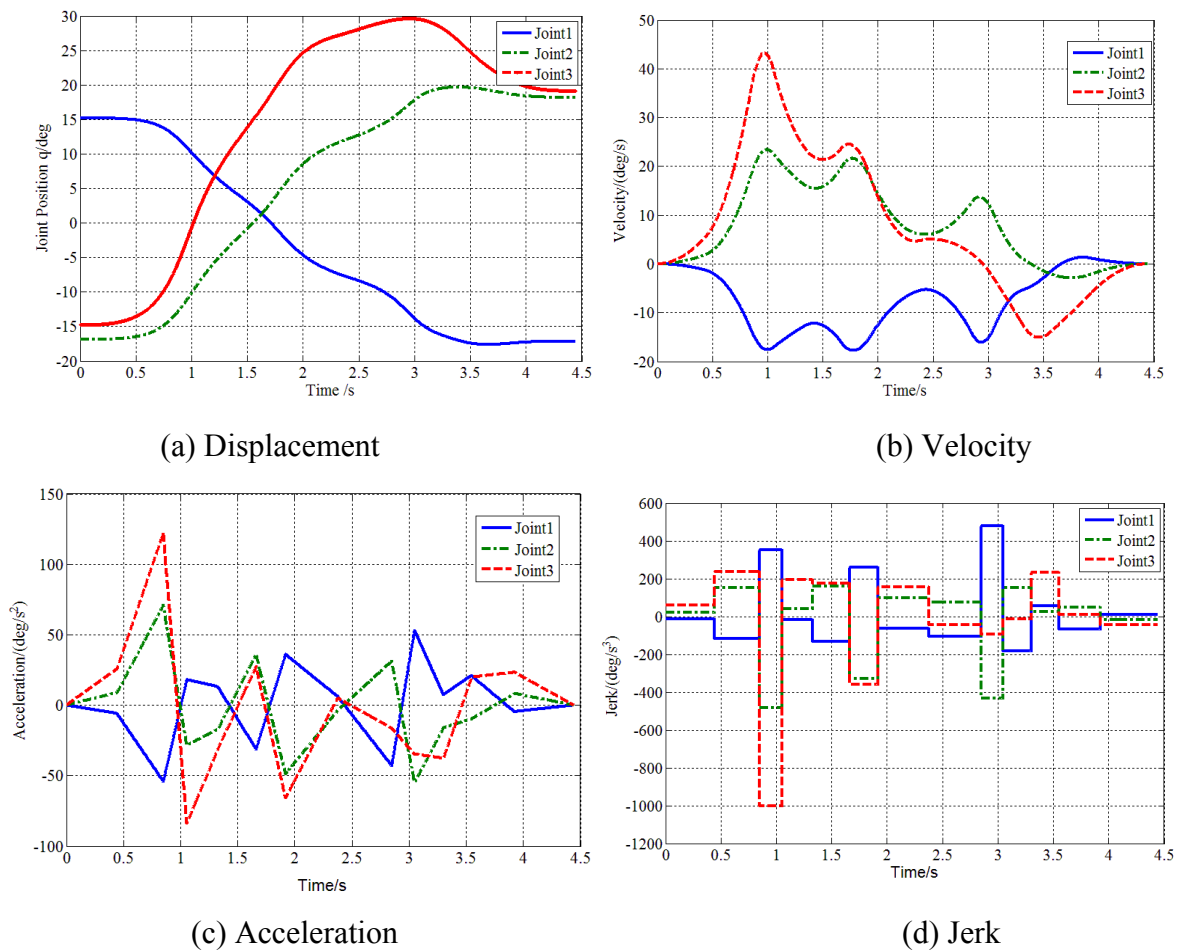


Figure 7. Displacement, velocity, and secondary acceleration of each joint, $W_T = 1$ and $W_J = 0$.

5.3. Experiment analyses

Aiming at the motion characteristics of the active joint of the MLM, the time-jerk motion trajectory planning problem is proposed in this paper. By setting its weight parameter, the time-jerk mobility parameter in its motion process is optimized. Firstly, simulation analysis was carried out for two states, $W_T = 1$ and $W_T = 0$. It can be found from Figures 7 and 8 that when $W_T = 1$, the trajectory planning time was less than 4.5 s, and the maximum jerk was 1000 deg/s^3 . When $W_T = 0$ and $W_J = 0$, the simulation time is 6 s and the maximum jerk degree is 68 deg/s^3 . Therefore, we need to find a good set of weight parameters so as to optimize the motion trajectory of the driving joint.

Table 5 shows that the shortest execution time is 2.9885 s, and as the time weighted coefficient values (W_T) decrease, the execution time of the MLM increase, and jerks of actuators decrease. That is to say, the reduction of the jerk is at the expense of the execution efficiency. When the value of W_T is less than 0.999999, the total value of maximum jerks of joints does not significantly decrease as exaction time increases. And when W_T is less than 0.9993, the total time taken to complete the motion trajectory by the MLM will be more than 5 s, which cannot meet the design requirements. When $W_T = 0.999995$ and $W_J = 0.000005$, the optimal solution is obtained at a certain extent. The results of the simulations are reported in Figures 9 and 10.

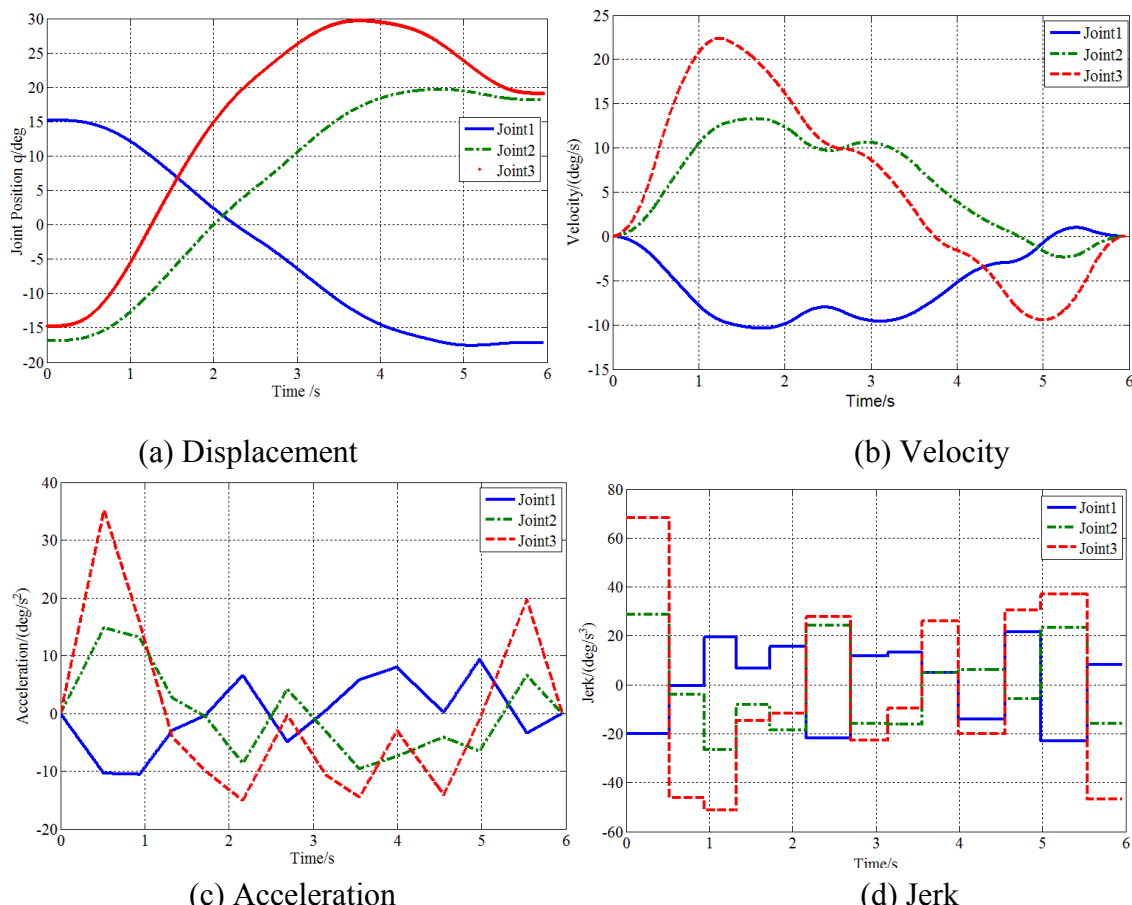
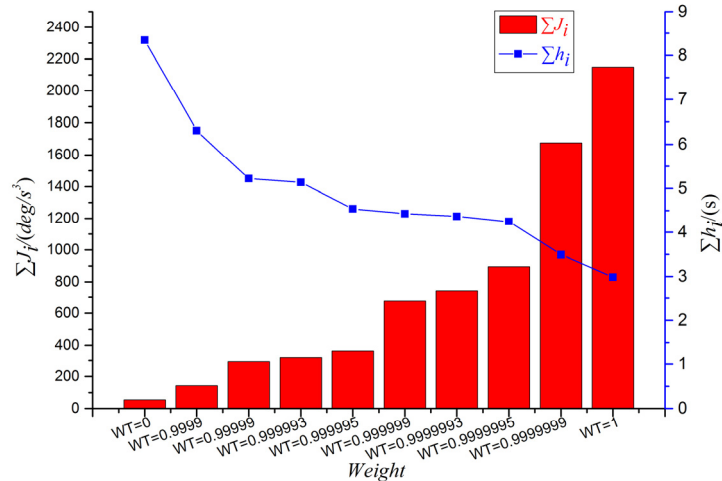


Figure 8. Displacement, velocity, acceleration and secondary acceleration of each joint, $W_T = 0$ and $W_J = 1$.

Table 5. Results of trajectory optimization.

Parameter	Weight									
	0	0.9999	0.99999	0.999993	0.999995	0.999999	0.9999993	0.9999995	0.9999999	1
W_T	0	0.9999	0.99999	0.999993	0.999995	0.999999	0.9999993	0.9999995	0.9999999	1
W_J	1	0.0001	0.00001	0.000007	0.000005	0.000001	0.0000097	0.0000005	0.0000001	0
h_1/s	0.6895	0.5237	0.4923	0.4077	0.3636	0.2280	0.3071	0.3035	0.2114	0.2418
h_2/s	0.6751	0.4432	0.3989	0.4267	0.3191	0.4687	0.3345	0.3438	0.2524	0.2096
h_3/s	0.6436	0.4758	0.3564	0.4078	0.3177	0.5041	0.3041	0.2955	0.3396	0.2456
h_4/s	0.5616	0.5045	0.3440	0.4342	0.3460	0.4956	0.3985	0.3276	0.2648	0.3534
h_5/s	0.5439	0.5671	0.4442	0.4231	0.3148	0.3607	0.3807	0.3877	0.3253	0.1002
h_6/s	0.5418	0.5636	0.4803	0.4363	0.3091	0.2937	0.3051	0.3808	0.2937	0.3269
h_7/s	0.4944	0.5098	0.3753	0.3980	0.3611	0.2710	0.4055	0.3192	0.2650	0.1699
h_8/s	0.6682	0.5053	0.4480	0.3968	0.3082	0.2635	0.3280	0.3406	0.2150	0.3597
h_9/s	0.6866	0.4408	0.5232	0.3425	0.3595	0.2364	0.3029	0.3233	0.2625	0.1181
h_{10}/s	0.6658	0.3565	0.3052	0.3344	0.3911	0.2460	0.3029	0.2986	0.2813	0.2749
h_{11}/s	0.5310	0.5236	0.2794	0.3448	0.3895	0.3448	0.3308	0.3078	0.2626	0.1813
h_9/s	0.8855	0.5927	0.3653	0.3674	0.3241	0.3714	0.3153	0.2651	0.2694	0.2019
h_{10}/s	0.8473	0.3004	0.4102	0.4171	0.4553	0.3442	0.3532	0.3571	0.2512	0.2051
$\sum h_i$	8.4343	6.3069	5.2227	5.1368	4.5591	4.4282	4.3687	4.2504	3.4944	2.9885
$J_{1\max}$	7.8279	31.4263	80.6735	69.6688	81.161	190.0436	204.8789	253.3385	552.7644	732.5254
$J_{2\max}$	5.9946	27.9385	82.6640	77.1002	84.0519	214.9931	238.5967	301.8268	548.4399	814.6972
$J_{3\max}$	40.9249	82.6025	129.6890	152.0706	138.8546	270.9026	296.1057	340.8264	575.4084	602.4032
$\sum J_i$	54.7474	141.9673	293.0265	298.8396	304.0675	675.9392	739.5813	895.9917	1676.6127	2149.6259

Note: h_i for the time intervals in seconds, $J_{1\max}$, $J_{2\max}$ and $J_{3\max}$ for the absolute values of maximum jerk of the joints 1–3, respectively, J_i for the total value of jerks (absolute values) of each joint.

**Figure 9.** Results of trajectory optimization.

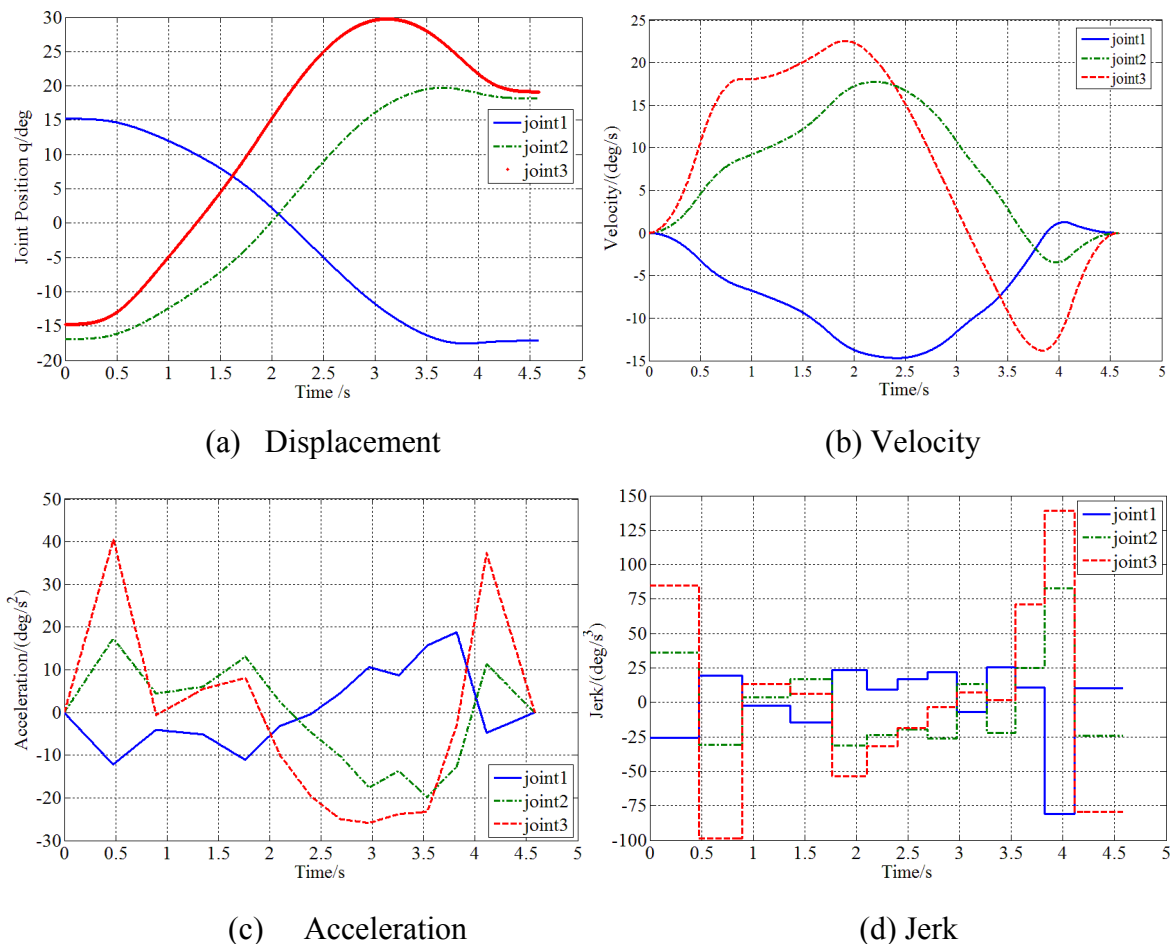


Figure 10. Displacement, velocity, acceleration and secondary acceleration of each joint.

The convergence of the algorithm is shown in Figure 11.

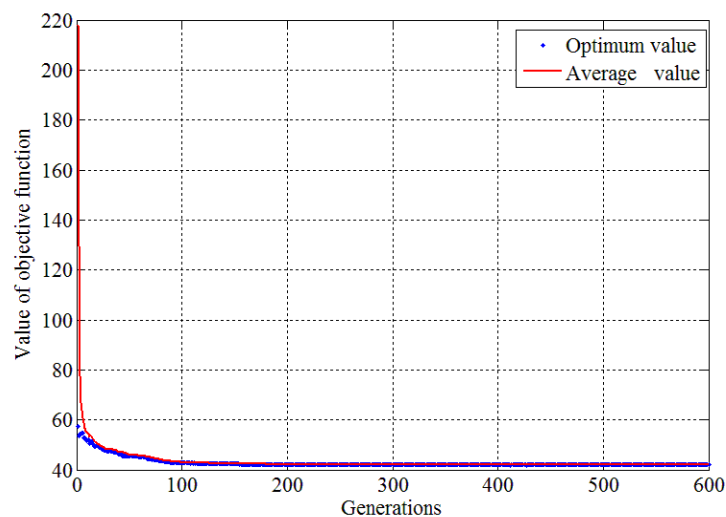


Figure 11. Algorithm convergence of AGA.

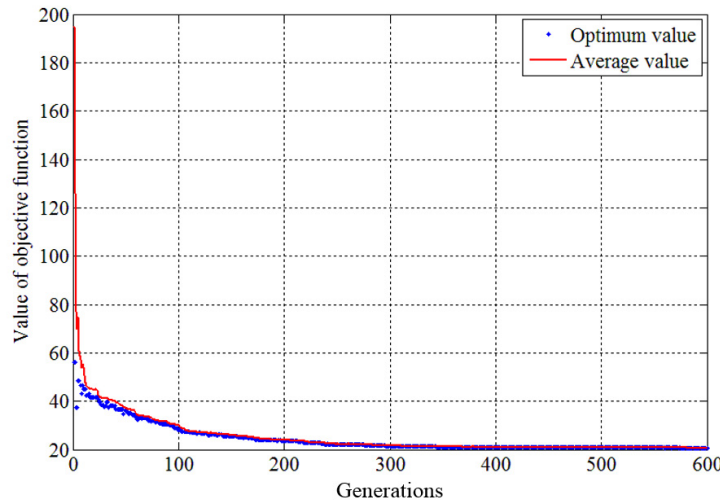


Figure 12. Algorithm convergence of GA.

It can be found from Figure 11 and Table 6 that the algorithm has a fast convergence speed, which is suitable for solving the optimal time-jerk problem and meeting the actual demand. In the experiment, in order to verify the effectiveness of the algorithm, GA and AGA were used to solve the optimal trajectory of MLM. The population size of each optimization algorithm was 50, and the number of iterations was 600. By comparing Figures 11 and 12, it is found that the convergence rate of the improved AGA is better than that of GA. And AGA has fewer values of objective function.

Table 6 compares the precocity and convergence performance of AGA and GA algorithms. The experiments were repeated 30 times, and the evolution algebra of both algorithms was 600 generations. It can be seen from the Table 6 that AGA has significantly improved its global optimization ability and fast convergence ability.

Table 6. Performance comparison between AGA and GA.

Comparative items	Converges to the global optimal solution times	Number of times of falling into the local optimal solution	Converges to the global optimal solution least algebra	Mean convergence generations
Arithmetic				
AGA	30	0	160	190
GA	9	18	240	260

6. Conclusions

In this paper, a novel mobile landing mechanism (MLM) is proposed. It realizes functions like landing on the lunar surface and walking in complex terrain environments, and greatly extends features of traditional landers. In order to verify the walking feasibility and reliability of the MLM. Firstly, the monte-Carlo method is used to solve the workspace, and the motion feasibility of the mechanism is verified. Secondly, combining with the constraints of velocity, acceleration and

secondary acceleration of each driving joint of the MLM, the trajectory of its joint space is planned by using cubic spline curve. And based on the weighted coefficient method, an optimal time-jerk pedestal trajectory planning model is established. Finally, by comparing the genetic algorithm (GA) with the adaptive genetic algorithm (AGA), an optimization algorithm is proposed to solve the joint trajectory optimization problem of the MLM, which can obtain better trajectory under constraints. Simulation shows that the motion performance of the mechanism is continuous and stable, which proves the rationality and effectiveness of the foot trajectory planning method.

Future work has several directions, such as: (1) as for the working space scope of the lander, further optimization is needed in the future to improve the motion performance of the lander. (2) the designed AGA for the weighted coefficient of time weighted coefficient and shock of optimal experimental method is used to approximate values, only to solve the approximate solution, and the lack of rigorous mathematical deduction, therefore, an optimization algorithm is designed to automatically obtain the global optimal solution of the objective function is a difficult problem to study for the future and goals. (3) The method in this paper can be extended and applied to a variety of series and parallel robots, so as to realize the motion capability of traditional robots.

Acknowledgments

The authors would like to thank team members in In-orbit control and landing laboratory of Nanjing University of Aeronautics. This work was funded by the National 13th Five-Year Civil Space Program [D030103], the National Natural Science Foundation (51675264) and the Youth Science and Technology Innovation Fund of Nanjing University of Aeronautics and Astronautics (NS2018052).

Conflict of interest

The authors declare no conflict of interest. The funders had no role in the design of the study; in the collection, analyses, or interpretation of data; in the writing of the manuscript, or in the decision to publish the results.

References

1. T. Okada, S. Sasaki, T. Sugihara, K. Saiki, H. Akiyama, M. Ohtake, et al., Lander and rover exploration on the lunar surface: A study for SELENE-B mission, *Adv. Space Res.*, **37** (2006), 88–92.
2. R. J. Williams, E. K. Gibson, The origin and stability of lunar goethite, hematite and magnetite, *Earth Planet. Sci. Lett.*, **17** (1972), 84–88.
3. T. E. Ford, C. Eng, A. F. R. Ae. S, The Apollo lunar module: a description of the construction of the lunar module used to make the first manned landing of a space vehicle on another planet, *Aircraft Eng. Aerosp. Technol.*, **41** (1969), 26–28.
4. R. Parkinson, The use of system models in the Euro Moon spacecraft design, *Acta Astronaut.*, **44** (1999), 437–443.

5. M. Benton, B. Donahue, D. Bienhoff, G. Caplin, D. Smith, K. Reiley, *Configuration Options to Maximize Lunar Surface Reuse of Altair Lander Structure and Systems*, AIAA SPACE 2009 Conference & Exposition, 2006.
6. M. A. Siegler, S. E. Smrekar, M. Grott, S. Piqueux, N. Mueller, J. Pierre, et al., The InSight Mars Lander and Its Effect on the Subsurface Thermal Environment, *Space Sci. Rev.*, **211** (2017), 1–17.
7. P. J. Ye, Z. Z. Sun, H. Zhang, F. Li, An overview of the mission and technical characteristics of change'4 lunar probe, *Sci. China Technol. Sci.*, **60** (2017), 658–667.
8. K. Iagnemma, H. Shibly, A. Rzepniewski, S. Dubowsky, P. Territories, *Planning and Control Algorithms for Enhanced Rough-Terrain Rover Mobility*, International Symposium on Artificial Intelligence, Robotics, and Automation in Space, 2001.
9. R. Lindemann, D. B. Bickler, B. D. Harrington, G. M. Ortiz, C. J. Voothees, Mars exploration rover mobility development-mechanical mobility hardware design, development, and testing, *IEEE Rob. Autom. Mag.*, **13** (2006), 19–26.
10. C. K. Liu, B. F. Wang, J. Wang, G. S. Tang, W. J. Wan, Y. L. Bu, Integrated INS and vision based orientation determination and positioning of CE-3 lunar rover, *J. Spacecr. TT&C Technol.*, **33** (2014), 250–257.
11. F. Cordes, F. Kirchner, A. Babu, Design and field testing of a rover with an actively articulated suspension system in a Mars analogy terrain, *J. Field Robo.*, **35** (2018), 1149–1181.
12. L. Liang, Z. Zhang, L. Guo, C. Yang, Y. Zeng, M. Li, et al., Mobile Lunar Lander Crewed Lunar Exploration Missions, *Man. Spaceflight*, **21** (2015), 472–478.
13. R. Zhu, Advances in the Soviet/Russian EVA Spacesuit Technology, *Man. Spaceflight*, **1** (2009), 25–45.
14. B. Birkenstaedt, J. Hopkins, B. Kutter, F. Zegler, T. Mosher, Lunar Lander Configurations Incorporating Accessibility, Mobility, and Centaur Cryogenic Propulsion Experience, *Space*, **2006** (2006), 1–12.
15. Q. Liang, D. Zhang, Y. Wang, G. Coppola, Y. Ge, PM based multi-component F/T sensors—State of the art and trends, *Robot. Robo. Comput. Integr. Manuf.*, **29** (2013), 1–7.
16. T. Hashimoto, T. Hoshino, S. Tanaka, M. Otsuki, H. Otake, H. Morimoto, Japanese moon lander SELENE2—Present status in 2009, *Acta Astronaut.*, **68** (2011), 1386–1391.
17. F. Pierrot, C. Reynaud, A. Fournier, DELTA: a simple and efficient parallel robot, *Robotica*, **8** (1990), 105–109.
18. V. Poppeová, V. Bulej, P. Šindler, *Development of simulation software and control system for mechanism with hybrid kinematic structure*, ISR 2010 (41st International Symposium on Robotics) and ROBOTIK 2010 (6th German Conference on Robotics), 2010.
19. G. Zhong, H. Deng, G. Xin, H. Wang, Dynamic hybrid control of a hexapod walking robot experimental verification, *IEEE Trans. Ind. Electron.*, **63** (2016), 5001–5011.
20. P. Yang, F. Gao, Leg kinematic analysis and prototype experiments of walking-operating multifunctional hexapod robot, *Proc. Inst. Mech. Eng. Part C*, **228** (2014), 2217–2232.
21. M. Dirik, A. F Kocamaz, O. Castillo, Global Path Planning and Path-Following for Wheeled Mobile Robot Using a Novel Control Structure Based on a Vision Sensor, *Int. J. Fuzzy Syst.*, **22** (2020), 1880–1890.
22. M. Dirik, O. Castillo, A. F. Kocamaz, Visual-Servoing Based Global Path Planning Using Interval Type-2 Fuzzy Logic Control, *Axioms*, **58** (2019), 1–16.

23. U. Orozco-Rosas, K. Picos, O. Montiel, Hybrid path planning algorithm based on membrane pseudo-bacterial potential field for autonomous mobile robots, *IEEE Access*, **7** (2019), 156787–156803.
24. O. Montiel, U. Orozco-Rosas, R. Sepúlveda, Path planning for mobile robots using Bacterial Potential Field for avoiding static and dynamic obstacles, *Expert Syst. Appl.*, **42** (2015), 5177–5191.
25. O. Montiel-Ross, R. Sepúlveda, O. Castillo, P. Melin, Ant colony test center for planning autonomous mobile robot navigation, *Comput. Appl. Eng. Educ.*, **21** (2013), 214–229.
26. M. A. Porta Garcia, O. Montiel, O. Castillo, R. Sepúlveda, P. Melin, Path planning for autonomous mobile robot navigation with ant colony optimization and fuzzy cost function evaluation, *Appl. Soft Comput.*, **9** (2009), 1102–1110.
27. Y. Pan, F. Gao, A new six-parallel-legged walking robot for drilling holes on the fuselage, *Proc. Inst. Mech. Eng., Part C*, **228** (2014), 753–764.
28. J. T. Yen, Y. H. Chang, Rate-dependent control strategies stabilize limb forces during human locomotion, *J. R. Soc. Interface*, **7** (2010), 801–810.
29. S. K. Banala, S. K. Agrawal, S. H. Kim, J. P. Scholz, Novel gait adaptation and neuromotor training results using an active leg exoskeleton, *IEEE-ASME Trans. Mechatron.*, **15** (2010), 216–225.
30. F. T. Cheng, H. L. Lee, D. E. Orin, *Increasing the locomotive stability margin of multilegged vehicles*, Proceedings 1999 IEEE International Conference on Robotics and Automation, 1999.
31. D. Pongas, M. Mistry, S. Schaal, *A robust quadruped walking gait for traversing rough terrain*, Proceedings 2007 IEEE International Conference on Robotics and Automation, 2007.
32. S. Zhang, X. Rong, Y. Li, B. Li, A composite cog trajectory planning method for the quadruped robot walking on rough terrain, *Int. J. Control. Autom.*, **8** (2015), 101–118.
33. H. Liu, X. Lai, W. Wu, Time-optimal and jerk-continuous trajectory planning for robot manipulators with kinematic constraints, *Robo. Comput. Integr. Manuf.*, **29** (2013), 309–317.
34. H. Xu, X. Xie, J. Zhuang, S. Wang, Global Time-energy Optimal Planning of Industrial Robot Trajectories, *J. Mech. Eng.*, **46** (2010), 19–25.
35. F. Liu, L. Fei, Time-jerk optimal planning of industrial robot trajectories, *Int. J. Robo. Autom.*, **31** (2016), 1–7.
36. S. F. P. Saramago, V. Steffen Jr, Optimization of the Trajectory Planning of Robot Manipulators Taking into Account the Dynamics of the System, *Mech. Mach. Theory*, **33** (1998), 883–894.
37. S. Wen, Z. Ma, S. Wen, Y. Zhao, J. Yao, *The study of NAO robot arm based on direct kinematics by using D-H method*, 2014 UKACC International Conference on Control (CONTROL), 2014.
38. Y. Guan, K. Yokoi, *Reachable Space Generation of A Humanoid Robot Using The Monte Carlo Method*, 2006 IEEE/RSJ International Conference on Intelligent Robots and Systems, 2006.
39. F. Liu, F. Lin, Time-jerk optimal planning of industrial robot trajectories, *Int. J. Robo. Autom.*, **31**, (2016), 1–7.
40. J. L. Martínez, J. González, J. Morales, A. Mandow, A. J. García-Cerezo, Mobile robot motion estimation by 2D scan matching with genetic and iterative closest point algorithms, *J. Field Robo.*, **23** (2010), 21–34.

